

Original article

Combined effects of permeability and fluid saturation on seismic wave dispersion and attenuation in partially-saturated sandstone

Qianqian Wei, Yang Wang[✉]*, De-hua Han, Min Sun, Qi Huang

Department of Earth and Atmospheric Sciences, University of Houston, Houston, Texas, USA

Keywords:

Low-frequency measurements
partial water saturation
bulk dispersion
bulk attenuation

Cited as:

Wei, Q., Wang, Y., Han, D., Sun, M., Huang, Q. Combined effects of permeability and fluid saturation on seismic wave dispersion and attenuation in partially-saturated sandstone. *Advances in Geo-Energy Research*, 2021, 5(2): 181-190, doi: 10.46690/ager.2021.02.07

Abstract:

Knowledge of dispersion and attenuation is essential for better reservoir characterization and hydrocarbon identification. However, limited by reliable laboratory data at seismic frequency bands, the roles of rock and fluid properties in inducing dispersion and attenuation are still poorly understood. Here we perform a series of laboratory measurements on two sandstones under both dry and partially water-saturated conditions at frequencies ranging from 2 to 600 Hz. Two samples, Bentheimer and Bandera sandstones, have similar porosity of ~20% but different permeability of 1830 mD and 33 mD. At vacuum-dry conditions, the bulk dispersion and attenuation in Bandera sandstone with more clay contents are distinctly larger than those in Bentheimer sandstone, suggesting clay contents might contribute to the inelasticity of the rock frame. The partially water-saturated results show the combined effects of rock permeability and fluid saturation on bulk dispersion and attenuation. Because of the high compressibility of gas, even a few percent of gas (~5%) can substantially dominate the pore-fluid relaxation by providing a quick and short communication path for pore pressure gradients. The consequent bulk dispersion and attenuation are negligible. However, when the sample is approaching a fully water-saturated condition (gas saturation <5%), the gas effect gradually decreases. Instead, the rock permeability begins to play an essential role in the pore-fluid relaxation. For Bandera sandstone with lower permeability, a partially relaxed status of pore fluids is achieved when the gas saturation is lower than 5%, accompanied by significant attenuation and dispersion.

1. Introduction

Porous rocks are normally saturated with multiphase fluids underground (Zhao et al., 2017; Li et al., 2020a). When seismic waves passing through such subsurface rocks, it is unavoidable to create dissipative and dispersive responses. Despite the presence of multiphase fluids, the seismic dissipation and dispersion are highly associated with the intrinsic rock permeability, which determines the fluid mobility inside the rocks (Batzle et al., 2006). As a result, it is of essential interest in investigating the combined effects of permeability and fluid saturation on the seismic wave dissipation and dispersion in porous sandstones, given their significance in hydrocarbon exploration and production, reservoir monitoring, and geothermal energy recovery (Goodway et al., 2012; Zhao et al., 2017; Ijeje et al., 2019).

It has been increasingly believed that the wave-induced fluid flow at different scales is primarily responsible for the seismic wave attenuation in fluid-saturated sedimentary rocks (Biot, 1956; White, 1975; O'Connell and Budiansky, 1977; Cleary, 1978; Mavko and Nur, 1979; Pride et al., 2004; Li et al., 2018; Müller et al., 2010). The wave-induced fluid flow occurs in the presence of pore pressure gradients, which is predominantly caused by the heterogeneities either in the rock matrix or in the saturating pore fluids. For this reason, rock physical parameters such as rock permeability, pore structure, fluid viscosity, as well as fluid distribution are expected to be sensitive to seismic wave attenuation (Zhao et al., 2017; Sarout et al., 2019). Effects of these parameters on dispersion and attenuation have been, to a certain degree, experimentally investigated in recent years (Murphy, 1982; Yin et al., 1992; Batzle et al., 2006; Tisato and Quintal, 2014; Chapman et

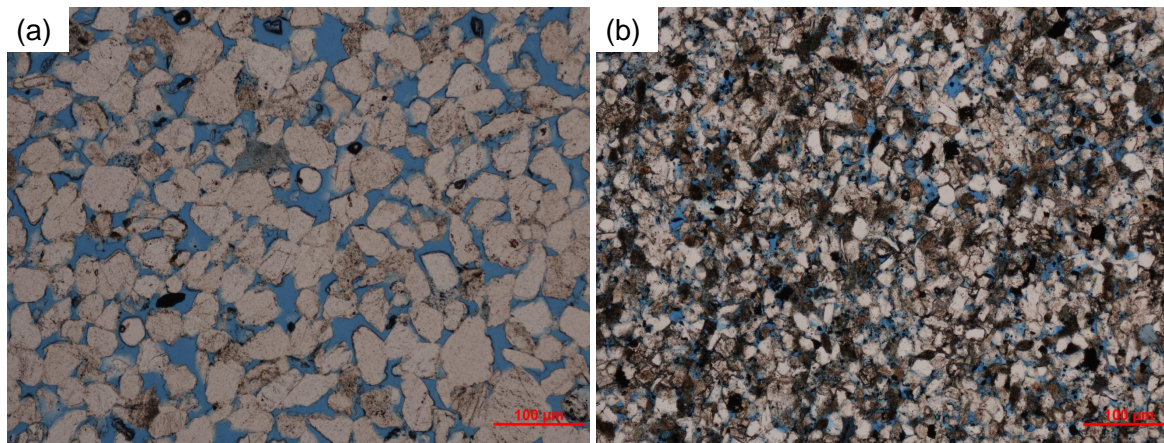


Fig. 1. Thin section images of Bentheimer (a) and Bandera (b) sandstone at the same scale (100 μm).

al., 2016; Spencer and Shine, 2016; Pimienta et al., 2017; Yin et al., 2019; Li et al., 2020b). Murphy (1982) and Yin et al. (1992) analyzed the effects of partial water saturation on the extensional attenuation in sandstone. The results suggest that significant attenuation occurs in the presence of a few percent of gas. Batzle et al. (2006) conducted low frequency measurements on tight sandstones and concluded that the rock permeability in conjunction with the fluid viscosity systematically affects the characteristic frequency of the P-wave relaxation. But they did not obtain the corresponding attenuation data. Pimienta et al. (2017) investigated frequency-dependent bulk modulus and attenuation in three sandstones with different permeability. They also found that the characteristic frequency of attenuation for each sandstone correlates well with its permeability. On the contrary, Spencer and Shine (2016)'s data illustrates that the relaxation of fluid-saturated sandstones shifts to a lower frequency range with the increase of fluid viscosity, but it does not show the dependence on permeability as predicted by Batzle et al. (2006) and Pimienta et al. (2017).

To date, limited researches have been done on experimentally investigating the dispersive and attenuative behaviors of porous rocks at seismic frequencies. Moreover, there exists a significant gap in explaining the existing seismic frequency data. Consequently, efforts must be made to precisely measure the dispersion and attenuation at seismic frequency bands and under varying physical conditions. Due to the high requirement of precision and the complexity of laboratory measurements, there are limited teams capable of conducting low-frequency measurements so far (Spencer, 1981; Batzle et al., 2006; Tisato and Quintal, 2013; Pimienta et al., 2015, 2019; Mikhaltsevitch et al., 2016; Li et al., 2020a). The most prospecting method in low-frequency measurements is the forced-oscillation technique, allowing measurements over a wide frequency range and under varying physical conditions. Spencer (1981) first performed the forced oscillation measurements with strain amplitude of approximately 10^{-6} at frequencies below 100 Hz for both dry and water-saturated sandstones. This technique is further developed by Batzle et al. (2006) and Adam et al. (2009), who obtained several sets of velocity and atten-

uation data by measuring various reservoir rock samples at seismic frequencies. Following the measurement principles as used by Batzle et al. (2006), a well-calibrated low-frequency measurement system has been developed in the Rock Physics Laboratory at the University of Houston (Li et al., 2020a), which is capable of measuring the elastic modulus and the corresponding attenuation of rocks under varying physical conditions at seismic frequency ranges (2-600 Hz).

This paper aims to further investigate the effects of rock permeability and fluid saturation on dispersion and attenuation in partially saturated sandstones at seismic frequencies. First, the experimental method and rock physical properties are described. Then, the frequency-dependent elastic properties are reported for both dry and partial saturated rocks. Ultimately, interpretations are suggested and discussed.

2. Experimental setups and methods

2.1 Sample descriptions

Two typical outcrop sandstones, Bentheimer and Bandera, are chosen to conduct low-frequency measurements. Two sandstone samples have similar porosity of $\sim 20\%$ but different permeabilities of 1830 mD and 33 mD. The mineral compositions of the two samples are characterized using the in-house X-ray diffraction (XRD) analysis, the results of which are shown in Table 1. Bentheimer sandstone is relatively clean, dominated by quartz with a volume fraction of 97.7%. In contrast, Bandera sandstone consists of a mixture of quartz (64.5%), plagioclase (17.1%), dolomite (10.8%), and clay (7.6%). The clay content in Bandera sandstone is visibly greater than that in Bentheimer sandstone. Meanwhile, the thin section images are taken under plane-polarized light to analyze the granular microstructures, as shown in Fig. 1. Solid grains in Bentheimer sandstone (Fig. 1(a)) are weakly cemented and well sorted. The grains are mainly rounded with an average radius of $\sim 100 \mu\text{m}$. The pore spaces, impregnated with blue epoxy, are homogeneously distributed and moderately well-interconnected. In Fig. 1(b), both grain and pore sizes of Bandera sandstone are smaller than those of Bentheimer sandstone. Solid grains are subangular or subrounded, mostly

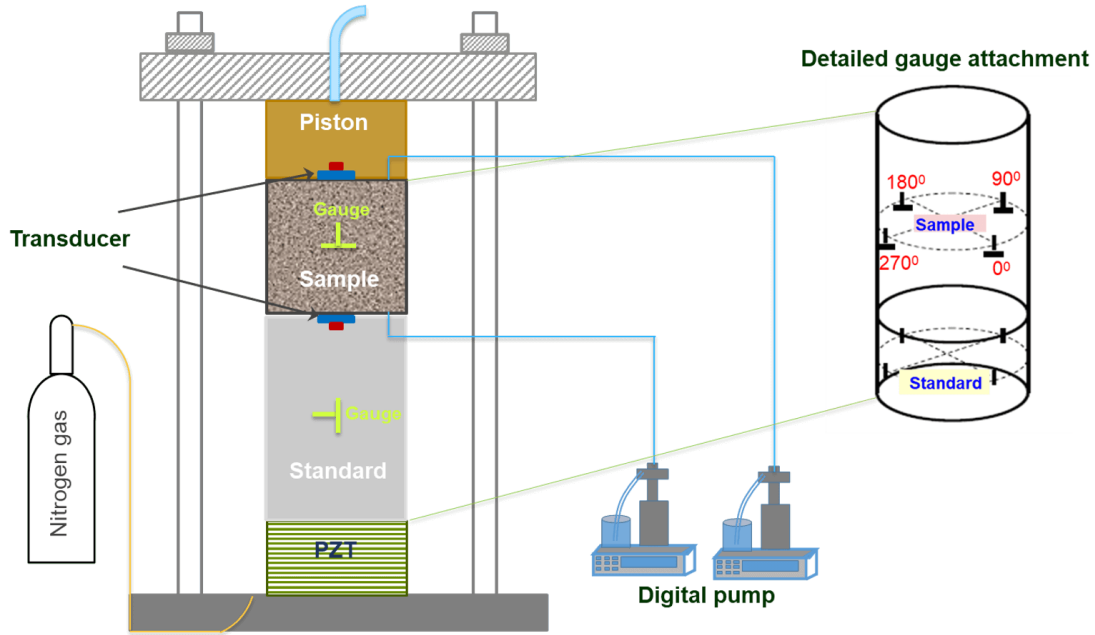


Fig. 2. Schematic of the low-frequency system based on the forced-oscillation method, modified after Li et al. (2020a, 2020b).

Table 1. Mineralogical compositions of two sandstone samples based on XRD analysis.

Sample	Quartz (wt.%)	Orthoclase (wt.%)	Plagioclase (wt.%)	Dolomite (wt.%)	Clay (wt.%)
Bentheimer	97.7	1.8	0	0	0.5
Bandera	64.5	0	17.1	10.8	7.6

cemented with argillaceous clay. Despite serving as cementation materials, some amounts of clay minerals fill the pore spaces, resulting in poor pore connectivity. Given the significant difference between the two sandstones in mineral compositions and pore connectivity, it is expected that there exist different dispersion and attenuation behaviors in the two samples.

2.2 Low-frequency system

Fig. 2 shows the schematic of our low-frequency system, which is based on the forced-oscillation method (Li et al., 2020a, 2020b). The key component is a column stacked by the rock sample, the aluminum standard, and the piezoelectric transducer (PZT) from top to bottom. PZT is one kind of ceramic material with a marked piezoelectric effect, namely, lead zirconated titanite. During the measurement, the function generator will first send out a continuous harmonic voltage wave with a specific frequency and amplitude. Then PZT is driven by the harmonic wave to apply sinusoidal-oscillated axial stress on the sample column. The rock sample and standard aluminum will be deformed by the vibration. The strain amplitudes are maintained at 10^{-7} , which is the same order of magnitude as seismic waves. Both axial and radial

strains are detected dynamically by the strain gauges attached to the samples' surfaces, as shown in Fig. 2. Notably, instead of measuring the applied stress directly, we use an aluminum standard as a reference to calculate the Young's modulus and the corresponding attenuation (Batzle et al., 2006). The aluminum standard is stacked with the sample under the same uniaxial stress. Meanwhile, the diameter of the standard is identical to that of the sample. Thus, the stress on the sample is almost the same as the stress on the standard. Then Young's modulus $E(\omega)$ and Poisson's ratio $\nu(\omega)$ of the rock sample can be calculated by comparing the strain amplitudes of the rock sample and the aluminum standard,

$$E(\omega) = \frac{E_{\perp}^{standard} * \varepsilon_{\perp}^{standard}(\omega)}{\varepsilon_{\perp}(\omega)} \quad (1)$$

$$\nu(\omega) = -\frac{\varepsilon_{\parallel}(\omega)}{\varepsilon_{\perp}(\omega)}$$

where $\varepsilon_{\perp}(\omega)$ and $\varepsilon_{\parallel}(\omega)$ are the axial and radial strains of the rock sample, respectively. $\varepsilon_{\perp}^{standard}(\omega)$ and $E_{\perp}^{standard}$ represent the axial strain and Young's modulus of the aluminum standard, respectively.

With the assumption of an isotropic and homogeneous medium, there exist two independent elastic parameters (Mavko et al., 2009). The two independent parameters, the bulk modulus $K(\omega)$ and shear modulus $G(\omega)$, could be calculated with the measured Young's modulus and Poisson's ratio as follows,

$$K(\omega) = \frac{E(\omega)}{3[1 - 2\nu(\omega)]} \quad (2)$$

$$G(\omega) = \frac{E(\omega)}{2[1 + \nu(\omega)]}$$

Together with the measured bulk density ρ , P-wave veloc-

ity $V_p(\omega)$ and S-wave velocity $V_s(\omega)$ can be obtained by,

$$\begin{aligned} V_p(\omega) &= \sqrt{\frac{K(\omega) + \frac{4}{3}G(\omega)}{\rho}} \\ V_s(\omega) &= \sqrt{\frac{G(\omega)}{\rho}} \end{aligned} \quad (3)$$

Additionally, the corresponding extensional attenuation can be inferred from the tangent of the phase difference θ between strains and stresses (O'Connell and Budiansky, 1977),

$$Q_E^{-1}(\omega) = \tan(\theta) \quad (4)$$

Since the aluminum is purely elastic from the first order, its strain is exactly in phase with the applied stress. Thus, we use the phase of strain on the standard aluminum to represent the phase of the applied stress (Batzle et al., 2006). The associated shear, P-wave, and bulk attenuation can be calculated throughout the following three equations:

$$Q_S^{-1}(\omega) = Q_E^{-1}(\omega) - \frac{\nu(\omega)}{1 + \nu(\omega)} Q_V^{-1}(\omega) \quad (5)$$

$$\begin{aligned} Q_P^{-1}(\omega) &= \frac{1 + \nu(\omega)}{[1 - \nu(\omega)][1 - 2\nu(\omega)]} Q_E^{-1}(\omega) \\ &\quad - \frac{2\nu(\omega)[2 - \nu(\omega)]}{[1 - 2\nu(\omega)]} Q_S^{-1}(\omega) \end{aligned} \quad (6)$$

$$Q_K^{-1}(\omega) = \frac{3}{1 - 2\nu(\omega)} Q_E^{-1}(\omega) - \frac{2[1 + \nu(\omega)]}{1 - 2\nu(\omega)} Q_S^{-1}(\omega) \quad (7)$$

where Q_K , Q_P , and Q_S are the bulk, P-wave, and shear quality factors, respectively.

Additionally, to obtain reliable low-frequency measurement data, calibrations of the low-frequency system are required prior to performing measurements on rock samples. Details of the calibration process and result can be found in Li et al. (2020a) using elastic aluminum and an attenuating Lucite. In general, the error for the dispersion is roughly 3%. The average error for the attenuation is ± 0.00035 .

2.3 Experimental procedures

The column assemblage in Fig. 2 is placed in a pressure vessel so that both confining pressure and pore pressure can be applied to the sample with separate controls. The confining pressure is supplied by a compressed nitrogen cylinder with a pressure regulator. The maximum pressure can be set as high as 42 MPa. The pore pressure is provided and controlled by a digital pump with various fluids desired for specific purposes. Meanwhile, the fluid saturation degree can be manipulated by precisely controlling the volume of the injected fluid. Therefore, the low-frequency system enables measurements at different pressures and fluid saturations.

Firstly, elastic properties of two samples are measured under the vacuum-dry condition at varied confining pressures (6.9 MPa, 13.8 MPa, and 20.7 MPa). Then we employ the imbibition method to inject water into the rock sample. The digital pump is used to manipulate the flow rate to precisely

quantify the water saturation degree ranging from 0% to 100%. During the measurements under different water saturations, the effective pressure is kept at a constant value of 20.7 MPa. Prior to achieving the fully water-saturated state (100%), the confining pressure and pore pressure are set as 20.8 MPa and 0.1 MPa, respectively. Once the sample is fully saturated, the pore pressure is increased up to 6.9 MPa, while the confining pressure is correspondingly set as 27.6 MPa. All measurements are conducted at room temperature.

3. Experimental results

3.1 Low-frequency data of dry samples

Fig. 3 shows the bulk modulus (K) and attenuation (Q_K^{-1}) as a function of the frequency ranging from 2 to 600 Hz under different confining pressures for two sandstone samples. Overall, at any confining pressure condition, the bulk modulus for Bentheimer sandstone almost keeps constant, whereas the bulk modulus for Bandera sandstone presents an increasing trend over the applied frequency range. In addition, as shown in Figs. 3(c) and 3(d), the bulk attenuation for Bentheimer sandstone is relatively tiny and almost independent of frequency. However, the bulk attenuation for Bandera sandstone is noticeable and increases with the increasing frequency. By comparing, both the bulk modulus and attenuation of Bandera sandstone are more sensitive to frequency than those of Bentheimer sandstone.

In Figs. 3(a) and 3(b), the bulk modulus of both samples increases with the increasing confining pressure. The increment with the confining pressure rising from 6.9 to 13.8 MPa is much larger than that with the confining pressure increasing from 13.8 to 20.7 MPa. In Figs. 3(c) and 3(d), the bulk attenuation is insensitive to the applied confining pressure for Bentheimer sandstone but decreases with the increasing confining pressure for Bandera sandstone, especially when the confining pressure increases from 6.9 to 13.8 MPa.

3.2 Low-frequency data of partially saturated samples

Fig. 4 shows the bulk modulus (K) and attenuation (Q_K^{-1}) of Bentheimer and Bandera sandstone as a function of the frequency at varying water saturation degrees. In the whole measurement, the effective pressure is kept at 20.7 MPa. In Fig. 4(a), the bulk modulus of Bentheimer sandstone almost remains constant over the applied frequency range, no matter what saturation state the sample is. However, the magnitude of the bulk modulus is dependent on the saturation degree. When Bentheimer sandstone changes from the vacuum-dry to partially saturated condition, the bulk modulus demonstrates a somewhat decreasing trend. However, as the water saturation approaches 100%, the bulk modulus jumps from ~ 11 GPa to ~ 15 GPa. Despite the effects of saturation degree, the bulk attenuation of Bentheimer sandstone is relatively tiny in the whole imbibition process, as shown in Fig. 4(c).

In contrast to Bentheimer sandstone, Bandera sandstone shows more complicated dispersion and attenuation behaviors, as shown in Figs. 4(b) and 4(d). In Fig. 4(b), the bulk

modulus of Bandera sandstone displays an increasing trend with the increasing frequency, indicating noticeable dispersion. The frequency-dependent bulk modulus is also associated with the saturation conditions. When the water saturation is below or equal to 93%, the bulk modulus dispersion is not noticeable until the frequency reaches 100 Hz. By further increasing water saturation to 95%, significant dispersion is

observed with a bulk modulus increment of ~ 3 GPa over the applied frequency range. With continued imbibition, the maximum dispersion is achieved at the water saturation level of 97%, accompanied by the bulk modulus increasing by 5.3 GPa. When the sample is fully saturated by water, there is a sharp increment in the magnitude of the bulk modulus, accompanied by a different frequency dependence. In contrast

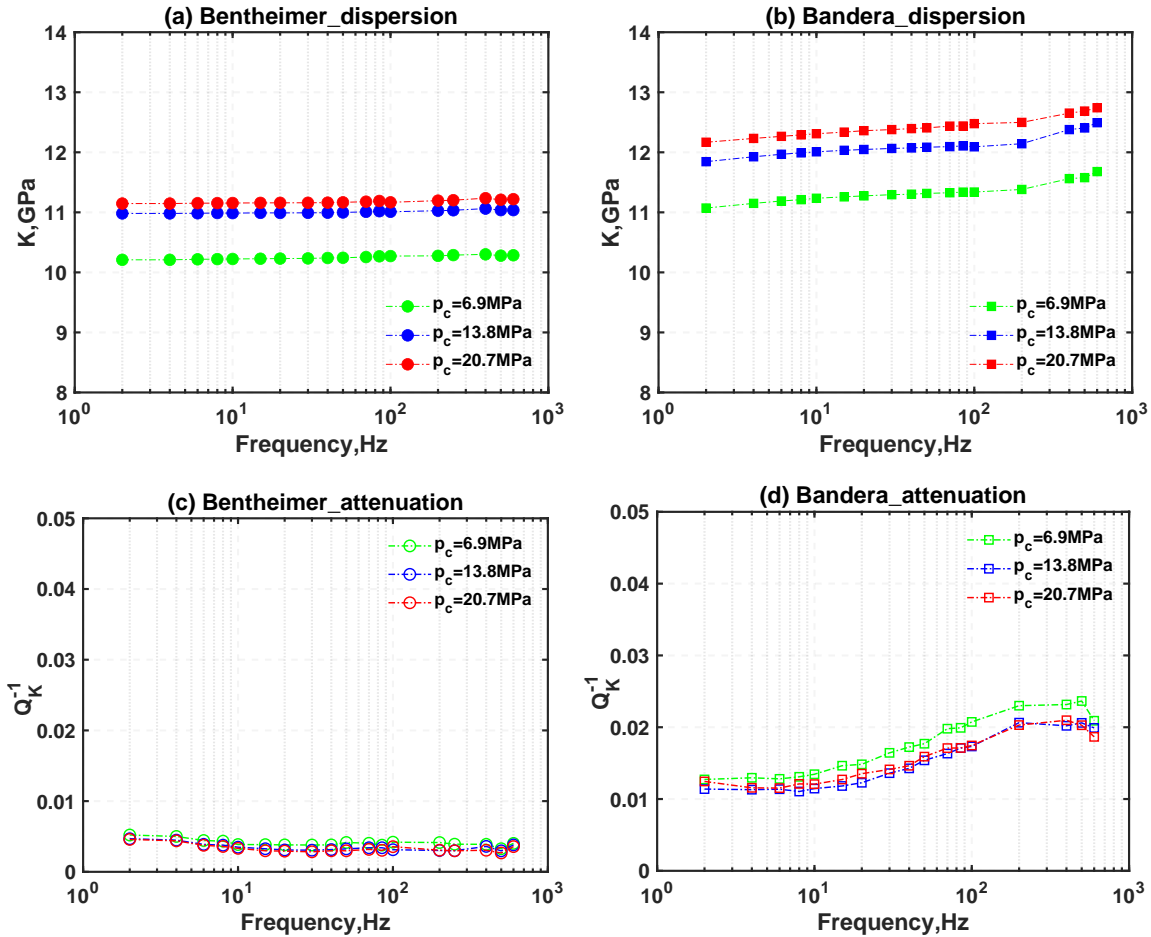
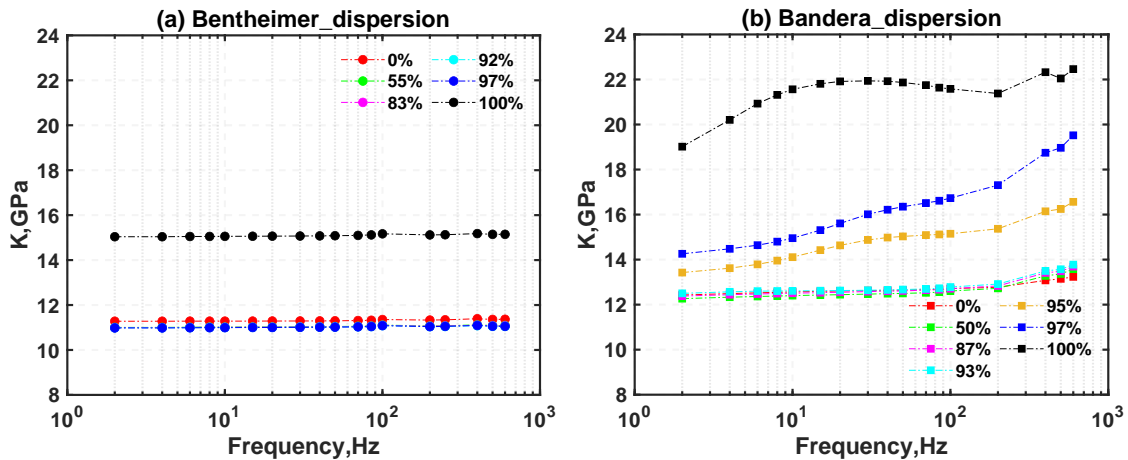


Fig. 3. The bulk modulus (K) as a function of the applied frequency for (a) dry Bentheimer and (b) dry Bandera sandstones; the bulk attenuation (Q_K^{-1}) for (c) dry Bentheimer and (d) dry Bandera sandstones.



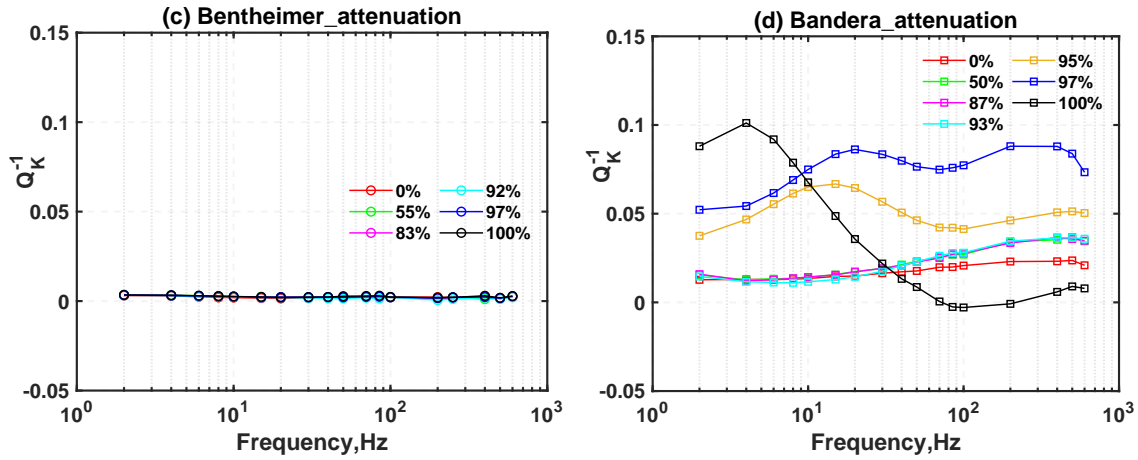


Fig. 4. The bulk modulus (K) as a function of the applied frequency at varying water saturation degrees for (a) Bentheimer and (b) Bandera sandstones; the bulk attenuation (Q_K^{-1}) for (c) Bentheimer and (d) Bandera sandstones.

to the dispersion at other saturation conditions, the dispersion zone at fully water saturation tends to move towards a lower frequency. In Fig. 4(d), Q_K^{-1} of Bandera sandstone shows a causal relationship with the dispersion behavior, namely, large dispersion correlates with high attenuation, and peak attenuation occurs at the point where the bulk modulus increases rapidly.

4. Discussion

4.1 Pressure and frequency dependence in dry samples

Data in Fig. 3 suggests that two dry samples exhibit similar pressure dependence of the bulk modulus and attenuation. The bulk modulus increases with the growing confining pressure, whereas the bulk attenuation has a trend to decrease with the increasing confining pressure, especially at relatively low-pressure levels. The pressure-dependent behavior might be attributed to the closure of soft pores or pre-existing cracks and the enlargement of grain-to-grain contacting area (Wang et al., 2020) when the confining pressure increases from 0 to 13.8 MPa. Subsequently, the rock becomes stiffer and stiffer, resulting in the increase of bulk modulus and the decrease of attenuation. When the confining pressure is beyond 13.8 MPa, compliant pores or grain contacts tend to have a weak impact on the bulk modulus. The bulk dispersion and attenuation subsequently are not sensitive to the increasing confining pressure.

For effects of the applied frequency, both dispersion and attenuation of the bulk modulus are pretty small in dry Bentheimer sandstone but are noticeable in dry Bandera sandstone, as seen in Fig. 3. The different frequency-dependent behaviors in two sandstones might be explained by their distinct mineral compositions, which would express elasticity or inelasticity. As stated by Heyliger et al. (2003) and Brown et al. (2016), from the first order, properties of solid minerals, like quartz or feldspar, are in accordance with the assumption of linear elasticity. As a result, Bentheimer sandstone, which is dominated by quartz (97.7%), to some extent, can be considered

as an elastic material, presenting quite small dispersion and attenuation. In contrast, besides the elastic minerals, there is an appreciable quantity of clay minerals (8%) in Bandera sandstone. The elastic properties of clay minerals are ambiguous due to the difficulties caused by their intrinsic properties. It is impossible to acquire a single clay crystal to measure its acoustic properties because of the small grain size of clay minerals. Meanwhile, the dispersion and attenuation caused by the viscous behavior of clay contents are seldom investigated either, especially at seismic frequency ranges. Klimentos and McCann (1990) investigated the relationship between attenuation and varying clay contents at 1 MHz in water-saturated sandstones. Their result suggests that the quality factor is inversely proportional to the increasing weight fraction of clay minerals. Based on their observation, we may propose that clay contents are responsible for the observed dispersion and attenuation of dry Bandera sandstone at seismic frequency.

4.2 Comparison of low-frequency data with Gassmann model

The well-known Gassmann equation (Gassmann, 1951) has been widely used to quantify the amount of the fluid effect in a homogeneous porous medium as follows,

$$\frac{K_{sat}}{K_0 - K_{sat}} = \frac{K_{dry}}{K_0 - K_{dry}} + \frac{K_{fl}}{\phi (K_0 - K_{fl})} \quad (8)$$

$$G_{sat} = G_{dry} \quad (9)$$

where K_{dry} is the effective bulk modulus of dry rock, K_{sat} represents the effective bulk modulus of fluid saturated rock, K_0 is the effective bulk modulus of rock minerals, K_{fl} is the effective bulk modulus of pore fluids, ϕ is the rock porosity, G_{sat} and G_{dry} are the shear modulus of fluid saturated rock and dry rock, respectively.

Gassmann's equation assumes that rock matrix is homogeneous and isotropic. Pore fluids have achieved an equilibrated state, giving rise to identical pore pressure inside the rock

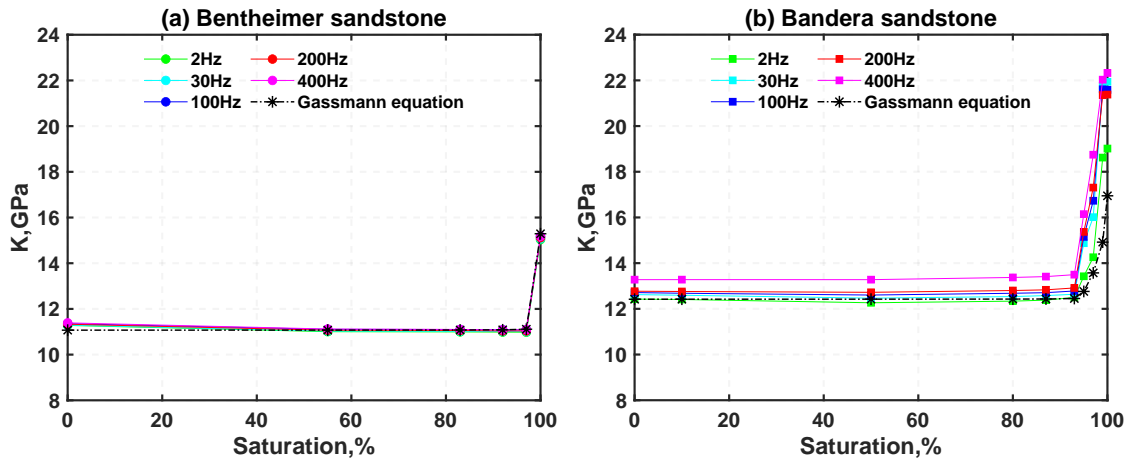


Fig. 5. Comparisons of the bulk modulus at seismic frequencies with that predicted by the Gassmann equation at different saturation conditions for (a) Bentheimer and (b) Bandera sandstone.

sample (Zhao et al., 2020). Therefore, it generally describes the lower bound of elastic moduli of a fluid-filled porous rock. Fig. 5 compares the bulk modulus at seismic frequencies with that predicted from the Gassmann equation for Bentheimer and Bandera sandstone, respectively. The bulk moduli of water and gas in the Gassmann equation are 2.25 GPa and 0.001 GPa (Mavko et al., 2009), respectively. Overall, for Bentheimer sandstone, Gassmann's estimation highly agrees with the measured seismic frequency data (Fig. 5(a)). This is caused by the fact that Bentheimer sandstone, with homogeneously distributed and well-interconnected pores, will have its pore fluid easily equilibrated within the measured frequency ranges (2-600 Hz). In this case, rock elastic properties can be represented by the Gassmann-Wood equations (Li et al., 2020b). For Bandera sandstone (Fig. 5(b)), when the water saturation is less than 93%, the measured bulk moduli at seismic frequencies match well with those predicted by the Gassmann equation. However, with further increasing water saturation, the bulk modulus exhibits noticeable dispersion, accompanied by an apparent deviation from the Gassmann estimation. Additionally, the deviation presents an increasing trend with the increasing frequency, as shown in Fig. 5(b). Considering the complicated pore structure of Bandera sandstone, the large dispersion is likely to be caused by the combined effects of rock permeability, gas saturation, and fluid-rock interaction.

4.3 Combined effects of rock permeability and gas saturation

The frequency-dependent behaviors of Bandera sandstone with partial water saturation, as shown in Figs. 4(b), 4(d), and 5(b), illustrate three pore-fluid statuses: relaxed, unrelaxed, and transition status (Mavko and Jizba, 1991; Batzle et al., 2006). The key parameter that dominates the pore-fluid status is the characteristic frequency, f_c , which can represent the relaxation time of the pore fluid. Considering the primary wave-induced fluid pressure diffusion taking place at mesoscopic scale, the corresponding characteristics frequency is expressed as (Pride

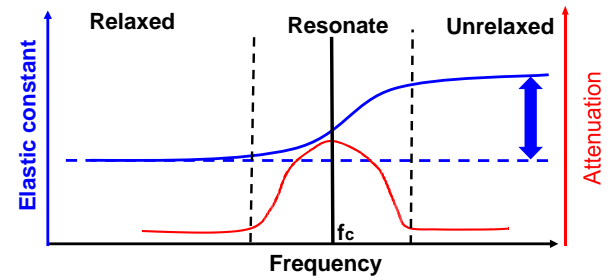


Fig. 6. A general feature of fluid-related dispersion and attenuation of elastic properties.

et al., 2004):

$$f_c = \frac{\kappa K_{fl}}{\eta L_c^2} \quad (10)$$

where κ is the permeability, K_{fl} is the fluid bulk modulus, η is the viscosity, and L_c is the critical fluid-diffusion relaxation scale. Fig. 6 shows the general feature of fluid-related wave dispersion and attenuation signatures based on the three typical fluid pressure relaxation status. On the one hand, when the measured frequency f is sufficiently lower than the rock's characteristic frequency f_c , the forced-oscillation induced pore pressure gradients would have enough time to completely equilibrate within the pore space and reach a relaxed status. In this case, the elastic modulus of the rock can be well predicted by the Gassmann-Wood equations. On the other hand, when the experimental frequency is much larger than f_c , the pore fluid will not have sufficient time to diffuse and remain in an unrelaxed status. In this case, the pore fluid is prone to increase the rock stiffness. In addition, there exists a transition zone from a relaxed to an unrelaxed status (Fig. 6), during which the pore pressure gradients will be partially equilibrated. As a result, a substantial change of elastic moduli can be obtained within the transition frequency ranges. Meanwhile, the oscillatory fluid flow resulting from unequilibrated pore pressures will consume the energy produced by the oscillated force, giving rise to apparent attenuation (Yin et al., 1992).

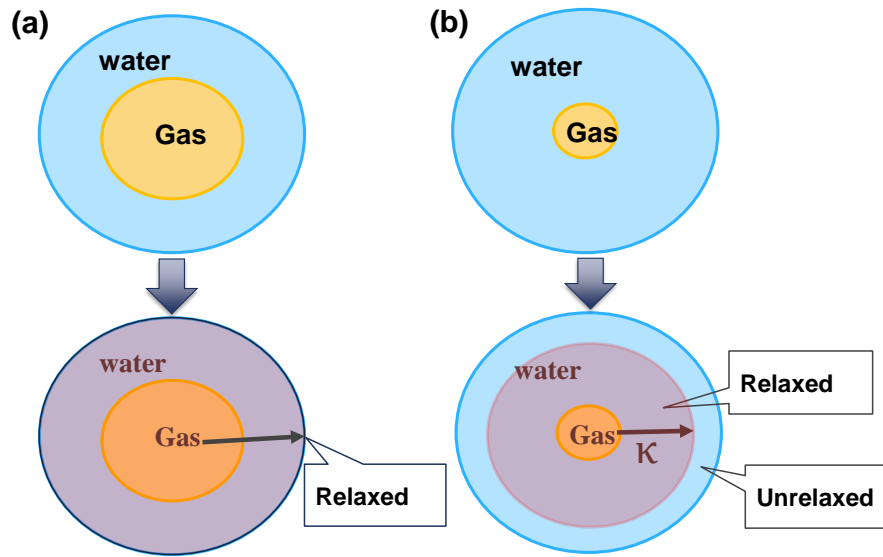


Fig. 7. Simple schematics to interpret the combined effects of rock permeability and gas saturation on the frequent-dependent behaviors of elastic moduli. The spherical gas-filled pocket is located at the center of the water-saturated sphere. (a) Gas saturation is larger than a certain percent of pore volume (e.g., 50%), pore fluid in a relaxed status; (b) gas saturation is less than a few percent of pore volume (e.g., 5%), pore fluid relaxation is largely dependent on rock permeability or pore connectivity.

Based on the above analysis, rock permeability and gas saturation associated with characteristic frequencies would play an important role in the frequent-dependent behaviors of elastic moduli. For simplicity, we use two schematics, as illustrated in Fig. 7, to qualitatively interpret our experimental observations. The spherical gas-filled pocket is located at the center of the water-saturated sphere. Since gas has extremely higher compressibility than water, a communication path for pore pressure gradients would be formed (White, 1975). When the gas saturation is larger than a certain percent of pore volume (e.g., 50%), as shown in Fig. 7(a), gas can substantially dominate pore fluid relaxation by providing a quick and short communication path for pore pressure gradients. Thus, the pore fluid can be relaxed quickly either in Bentheimer or Bandera sandstone, resulting in negligible dispersion and attenuation at the measured frequency range, as shown in Fig. 4. In Fig. 7(b), when the gas saturation is less than a few percent of pore volume (e.g., 5%), the gas effect would gradually decrease. The rock frame properties are expected to play important roles in the pore fluid relaxation. For the case of Bentheimer sandstone with higher permeability and better pore connectivity, the pore fluid can easily reach a relaxed status even though only 3% gas occupies the pore space, resulting in small attenuation and dispersion in Figs. 5(a) and 5(c). In contrast, for Bandera sandstone with lower permeability and poor pore connectivity, gas-water communication becomes difficult. As a result, pore pressure gradients need more time to reach an equilibrated state. At the applied frequency ranges, only parts of the pore fluid can reach a relaxed status. Therefore, in Figs. 5(b) and 5(d), when the water saturation is 95% or 97%, distinct bulk attenuation and dispersion can be observed.

The strain amplitude of a propagating seismic wave is typically limited to 10^{-7} - 10^{-6} , while the frequency ranges

between 10 and 100 Hz (Fjær, 2019). The corresponding wavelength falls into tens to hundreds of meters, which restricts the direction measurements of seismic velocities in the laboratory conditions. The forced deformation method provides an alternative approach to measure rock elastic properties using cm-scale core samples. From one aspect, the observations in this study give direct proof of that wave dispersion and attenuation are associated to rock permeability and fluid properties. From the other aspect, the laboratory low frequency measurements can be used to calibrate the seismic-well tie and seismic inversions, which will facilitate the hydrocarbon identification, high-permeability zone detection, and reservoir production monitoring.

5. Conclusions

In this study, a series of low-frequency measurements are performed on two sandstones with different permeability to investigate the roles of rock permeability and gas saturation in bulk dispersion and attenuation. The experiments are conducted at frequencies ranging from 2 Hz to 600 Hz under both vacuum-dry and partially water-saturated conditions. At vacuum-dry conditions, the bulk dispersion and attenuation in Bandera sandstone with more clay contents are distinctly larger than those in Bentheimer sandstone, suggesting clay contents might contribute to the inelasticity of the rock frame.

At partially water-saturated conditions, the bulk dispersion and attenuation in Bentheimer sandstone are relatively small in the whole imbibition process. The bulk modulus predicted by the Gassmann equation highly agrees with that measured at seismic frequencies, suggesting that a relaxed status of pore fluids is reached for the partially saturated Bentheimer sandstone. By comparing, Bandera sandstone shows complicated dispersion and attenuation behaviors. When the water saturation is below 93%, bulk dispersion and attenuation

are not noticeable. However, when the water saturation is beyond 93%, bulk dispersion and attenuation become significant, accompanied by apparent bulk modulus deviations from Gassmann's estimations. The mismatching between the measured data and the Gassmann prediction can be attributed to the combined effects of rock permeability and fluid saturation. As gas saturation is larger than a few percent ($\sim 5\%$), gas with relatively high compressibility dominates the pore-fluid relaxation by providing a quick and short communication path for pore pressure gradients. As a result, dispersion and attenuation are not significant when the water saturation is below 95%. With continued water injection, the gas effect gradually decreases. The rock permeability begins to dominate the pore-fluid relaxation. For Bandera sandstone with relatively low permeability, a partially relaxed status is reached with apparent attenuation and dispersion.

Acknowledgement

This work was supported by the Fluids/DHI consortium at the University of Houston.

Conflict of interest

The authors declare no competing interest.

Open Access This article is distributed under the terms and conditions of the Creative Commons Attribution (CC BY-NC-ND) license, which permits unrestricted use, distribution, and reproduction in any medium, provided the original work is properly cited.

References

- Adam, L., Batzle, M. L., Lewallen K. T. Seismic wave attenuation in carbonates. *Journal of Geophysical Research: Solid Earth*, 2009, 114: B06208.
- Batzle, M. L., Han, D. H., Hofmann, R. Fluid mobility and frequency-dependent seismic velocity-Direct measurements. *Geophysics*, 2006, 71(1): N1-N9.
- Biot, M. A. Theory of propagation of elastic waves in a fluid-saturated porous solid: II-Higher frequency range. *Journal of the Acoustic Society of America*, 1956, 28: 179-191.
- Brown, J. M., Angel, R. J., Ross, N. L. Elasticity of plagioclase feldspars. *Journal of Geophysical Research: Solid Earth*, 2016, 121: 663-675.
- Chapman, S., Tisato, N., Quintal, B., et al. Seismic attenuation in partially saturated Berea sandstone submitted to a range of confining pressures. *Journal of Geophysical Research: Solid Earth*, 2016, 121: 1664-1676.
- Cleary, M. P. Elastic and dynamic response regimes of fluid-impregnated solids with diverse microstructures. *International Journal of Solids and Structures*, 1978, 14(10): 795-819.
- Fjær, E. Relations between static and dynamic moduli of sedimentary rocks. *Geophysical Prospecting*, 2019, 67(1): 128-139.
- Gassmann, F. *Über die Elastizität poröser Medien*. *Veierteljahrsschrift der Naturforschenden Gesellschaft in Zürich*, 1951, 96: 1-23.
- Goodway, B., Monk, D., Perez, M., et al. Combined microseismic and 4D to calibrate and confirm surface 3D azimuthal AVO/LMR predictions of completions performance and well production in the Horn River gas shales of NEBC. *The Leading Edge*, 2012, 31(12): 1502-1511.
- Heyliger, P., Ledbetter, H., Kim, S. Elastic constants of natural quartz. *Journal of Acoustics Society of America*, 2003, 114(2): 644-650.
- Ijeje, J. J., Gan, Q., Cai, J. Influence of permeability anisotropy on heat transfer and permeability evolution in geothermal reservoir, *Advances in Geo-Energy Research*, 2019, 3: 43-51.
- Klimentos, T., McCann, C. Relationships among compressional wave attenuation, porosity, clay content, and permeability in sandstones. *Geophysics*, 1990, 55: 998-1014.
- Li, H., Wang, D., Gao, J., et al. Role of saturation on elastic dispersion and attenuation of tight rocks: An experimental study. *Journal of Geophysical Research: Solid Earth*, 2020a, 125(4): e2019JB018513.
- Li, H., Zhao, L., Han, D. H., et al. Experimental study on frequency-dependent elastic properties of weakly consolidated marine sandstone: Effects of partial saturation. *Geophysical Prospecting*, 2020b, 68(9): 2808-2824.
- Li, Z., Duan, Y., Fang, Q., et al. A study of relative permeability for transient two-phase flow in a low permeability fractal porous medium. *Advances in Geo-Energy Research*, 2018, 2(4): 369-379.
- Mavko, G., Mukerji, T., Dvorkin, J. *The Rock Physics Handbook*. Cambridge, UK, Cambridge University Press, 2009.
- Mavko, G., Nur, A. Wave attenuation in partially saturated rocks. *Geophysics*, 1979, 44: 161-178.
- Mavko, G., Jizba, D. Estimating grain-scale fluid effects on velocity dispersion in rocks. *Geophysics*, 1991, 56: 1940-1949.
- Mikhaltsevitch, V., Lebedev, M., Gurevich, B. Laboratory measurements of the effect of fluid saturation on elastic properties of carbonates at seismic frequencies. *Geophysical Prospecting*, 2016, 64(4): 799-809.
- Murphy, M. Effects of partial water saturation on attenuation in Massillon sandstone and Vycor porous glass. *The Journal of Acoustical Society of America*, 1982, 71(6): 1458-1468.
- Müller, T. M., Gurevich, B., Lebedev, M. Seismic wave attenuation and dispersion resulting from wave-induced flow in porous rocks-A review. *Geophysics*, 2010, 75: A147-A164.
- O'Connell, R. J., Budiansky, B. Viscoelastic properties of fluid-saturated cracked solids. *Journal of Geophysical Research*, 1977, 82: 5719-5740.
- Pimienta, L., Borgomano, J. V. M., Fortin, J., et al. Elastic dispersion and attenuation in fully saturated sandstones: Role of mineral content, porosity, and pressures. *Journal of Geophysical Research: Solid Earth*, 2017, 122: 9950-9965.
- Pimienta, L., David, C., Sarout, J., et al. Evolution in seismic properties during low and intermediate water saturation: Competing mechanisms during water imbibition? *Geo-*

- physical Research Letters, 2019, 46(9): 4581-4590.
- Pimienta, L., Fortin, J., Guéguen, Y. Bulk modulus dispersion and attenuation in sandstones. *Geophysics*, 2015, 80(2): D111-D127.
- Pride, S. R., Berryman, J. G., Harris, J. M. Seismic attenuation due to wave-induced flow. *Journal of Geophysical Research*, 2004, 109: B01201.
- Sarout, J., David, C., Pimienta, L. Seismic and microseismic signatures of fluids in rocks: Bridging the scale gap. *Journal of Geophysical Research: Solid Earth*, 2019, 124: 5379-5386.
- Spencer, J. W. Stress relaxations at low frequencies in fluid saturated rocks: Attenuation and modulus dispersion. *Journal of Geophysical Research: Solid Earth*, 1981, 42(C5): 1175-1180.
- Spencer, J. W., Shine, J. Seismic wave attenuation and modulus dispersion in sandstones. *Geophysics*, 2016, 81(3): D211-D231.
- Tisato, N., Quintal, B. Measurements of seismic attenuation and transient fluid pressure in partially saturated Berea sandstone: Evidence of fluid flow on the mesoscopic scale. *Geophysical Journal International*, 2013, 195: 342-351.
- Tisato, N., Quintal, B. Laboratory measurements of seismic attenuation in sandstone: Strain versus fluid saturation effects. *Geophysics*, 2014, 79: WB9-WB14.
- Wang, Y., Zhao, L., Han, D. H., et al. Micro-mechanical analysis of the effects of stress cycles on the dynamic and static mechanical properties of sandstone. *International Journal of Rock Mechanics and Mining Sciences*, 2020, 134: 104431.
- Yin, C. S., Batzle, M. L., Smith, B. J. Effects of partial liquid/gas saturation on extensional wave attenuation in Berea sandstone. *Geophysical Research Letters*, 1992, 19: 1399-1402.
- Yin, H., Borgomano, J. V. M., Wang, S., et al. Fluid substitution and shear weakening in clay-bearing sandstone at seismic frequencies. *Journal of Geophysical Research: Solid Earth*, 2019, 124: 1254-1272.
- Zhao, L., Cao, C., Yao, Q., et al. Gassmann consistency for different inclusion-based effective medium theories: Implications for elastic interactions and poroelasticity. *Journal of Geophysical Research: Solid Earth*, 2020, 125(3): e2019JB018328.
- Zhao, L., Yuan, H., Yang, J., et al. Mobility effect on poroelastic seismic signatures in partially saturated rocks with applications in time-lapse monitoring of a heavy oil reservoir. *Journal of Geophysical Research: Solid Earth*, 2017, 122: 8872-8891.